Bioelectromagnetics 41:21–33 (2020)

Multifrequency Analysis of Single Inductive Coil Measurements Across a Gel Phantom Simulation of Internal Bleeding in the Brain

Moshe Oziel,[1] Mohammad Hjouj,[2] Boris Rubinsky,[3] and Rafi Korenstein[1]*

[1]*Department of Physiology and Pharmacology, Tel-Aviv University, Tel-Aviv, Israel*
[2]*Department of Medical Imaging, Al-Quds University, Abu Dis, Palestine*
[3]*Department of Mechanical Engineering, University of California at Berkeley, Berkeley, California*

The present study is part of an ongoing effort to develop a simple diagnostic technology for detecting internal bleeding in the brain, which can be used in lieu or in support of medical imaging and thereby reduce the cost of diagnostics in general, and in particular, would make diagnostics accessible to economically disadvantaged populations. The study deals with a single coil inductive device to be used for detecting cerebral hemorrhage. It presents a first-order experimental study that examines the predictions of our recently published theoretical study. The experimental model employs a homogeneous cylindrical phantom in which internal head bleeding was simulated by way of a fluid inclusion. We measured the changes in amplitude and phase across the coil with a network vector analyzer as a function of frequency (100–1,000 MHz), volume of blood simulating fluid, and the site of the fluid injection. We have developed a new mathematical model to statistically analyze the complex data produced in this experiment. We determined that the resolution for the fluid volume increase following fluid injection is strongly dependent on frequency as well as the location of liquid accumulation. The experimental data obtained in this study supports the predictions of our previous theoretical study, and the statistical analysis shows that the simple single coil device is sensitive enough to detect changes due to fluid volume alteration of two milliliters. Bioelectromagnetics. 2020;41:21–33. © 2019 Bioelectromagnetics Society

Keywords: hematoma; monitoring; non-contact; radio frequency; inductive coil

INTRODUCTION

Stroke is the second leading cause of death and the third leading cause of debilitating injury in the world [Geneva World Health Organization Estimates, 2016]. Approximately 10% to 20% of strokes are associated with intracerebral hemorrhage (ICH). About 40% of patients die in the first month following a stroke and 54% die during the first year. Only 12% to 39% of survivors retain long-term physiological function [An et al., 2017]. A case of ICH occurs every 18 min in the United States, with 15% of those suffering from subarachnoid aneurysmal hemorrhage (SAH), dying before arrival to the hospital. Of those arriving to the hospital, 25% will endure either a mistaken diagnosis or avoidable delays in treatment [Foundation Brain Aneurism, 2018]. The volume of hematoma can vary significantly, depending on the type and location of the bleeding. For example, intraparenchymal hemorrhages have a mean volume of 68.7 ml in a range of 0–200 ml [Caceres and Goldstein, 2012] while intraventricular hemorrhages have a range of 0–20 ml [Gebel et al., 1998]. ICH is an acute health problem, with a high percentage of death and incapacitation, which could be alleviated by rapid and reliable diagnosis [Foundation Brain Aneurism, 2018].

Medical imaging techniques such as magnetic resonance imaging, computerized tomography (CT), and Doppler ultrasound are the gold standards for the detection and diagnosis of internal bleeding in the brain [Huisman, 2005]. However, these technologies are expensive and require trained experts. In many parts of the world, including industrialized countries, the economically disadvantaged population has no access to these technologies [González et al., 2010]. Furthermore, these advanced diagnostic modalities

Conflict of Interest: None.

*Correspondence to: Rafi Korenstein, Department of Physiology and Pharmacology, Tel-Aviv University, PO Box 39040, Tel Aviv 69978, Israel. E-mail: korens@post.tau.ac.il

Received for review 22 February 2019; Accepted 24 October 2019

DOI:10.1002/bem.22230
Published online 21 November 2019 in Wiley Online Library (wileyonlinelibrary.com).

cannot be used in ambulances or for continuous monitoring of the brain in a hospital setting, where CT is contraindicated for children [Little, 2008].

Since the skull is rigid and the volume of the brain cavity is fixed, the physiological consequence of internal bleeding in the brain is a change in the ratio between the volume occupied by blood and cerebrospinal fluid (CSF), and the volume occupied by tissue. Because the dielectric properties of brain tissue, CSF, and blood are substantially different from each other [Nyboer, 1970; Foster and Schwan, 1989; Gabriel, 2000], changes in the fluid/brain tissue ratio in the brain can affect the electromagnetic properties of the brain. This has led to the use of non-contact electromagnetic measurements to detect or image [Mobashsher and Abbosh, 2016] changes in the fluid/tissue ratio inside the skull [e.g. Lin and Clarke, 1982; Clarke and Lin, 1983; Scharfetter et al., 1999; Griffiths et al., 1999; Qureshi et al., 2018]. Motivated by the medical needs of the economically disadvantaged population in Mexico, our group began developing simple and inexpensive diagnostic technologies for the detection of internal bleeding in the body with non-contact electromagnetic measurements [González and Rubinsky, 2006]. The technology referred to as "Volumetric Integral Phase-Shift Spectroscopy" (VIPS) employs measurements of the changes in the amplitude and phase of electromagnetic waves transmitted across the bulk of the brain over a range of frequencies. Our VIPS technology has received CE and U.S. Food and Drug Administration (FDA) approval and is currently used in a variety of clinical studies such as for the development of classifiers to detect edema and hematoma [González et al., 2013], as a tool to study cerebrovascular reactivity [Oziel et al., 2016], or to detect fluid shifts in the brain during dialysis [Rao et al., 2018].

VIPS technology is sensitive to changes in the distance between the coils across the head and to motion artifacts between the coils and the head. While this sensitivity to motion artifacts is not detrimental with patients who are unconscious, it is an impediment to long-term use with patients who are alert. To overcome the sensitivity of the VIPS system to motion artifacts, we have developed two new devices, as described in Oziel et al. [2017, 2018]. The primary application of these devices is to detect changes in the volume of a hematoma in the head using inexpensive and simple technology. One of these technologies is based on the principles of radar [Oziel et al., 2017] and employs one antenna to detect changes in the fluid/brain tissue ratio in the brain. The second employs a single inductive coil around the head [Oziel et al., 2018]. These technologies are less sensitive to the motion of the head relative to the transmission device than the earlier VIPS two-coil system [González and Rubinsky, 2006]. The use of one antenna/coil to measure changes in electromagnetic properties in an object of interest is not novel; it is used extensively in industry for non-invasive measurements of solid objects [Wadley and Choi, 1997] and in medicine for such applications as non-contact measurements of breathing [Teichmann et al., 2013, 2014] and thermal therapy monitoring [Haynes et al., 2014].

We previously appraised the effect of changes in the fluid/brain tissue ratio on the impedance in the frequency range from 100 MHz to 1 GHz [Oziel et al., 2017, 2018]. A numerical solution (Comsol Multiphysics, COMSOL, Stockholm, Sweden) of the complete Maxwell equations in the head, their surroundings, and the antenna was obtained. In Oziel et al. [2017], we analyzed the changes in impedance of a spiral antenna backed by a reflector plate, facing different parts of the head relative to a hematoma in the brain. In Oziel et al. [2018], we examined by simulation the changes in the impedance of a coil surrounding the head, due to the formation of a hematoma. The analysis shows that when the location of the hematoma is not known, the coil antenna is advantageous over the spiral antenna in terms of ease of use and resolution. Several additional findings emerged from the analysis. The numerical analysis indicated that both antennas were sensitive enough to detect changes in blood volume as small as 2 ml. Another important finding was that the resolution is frequency-dependent and that the measurements must be performed over a wide range of frequencies. The observation that multiple frequency measurements are needed to analyze and detect changes in the blood volume/tissue ratio is consistent with our analytical and experimental observations with the two-coil VIPS devices [González and Rubinsky, 2006; González et al., 2013].

This study considers a simple experimental phantom made by a homogeneous cylinder with fluid inclusions to simulate internal bleeding in the brain and follows our previous theoretical study [Oziel et al., 2018]. The goal of this study was to experimentally verify the conclusions of the theoretical study [Oziel et al., 2018], namely that the single inductive coil measurements are sensitive enough to detect changes in blood volume in the head and that the sensitivity of the measurements is frequency-dependent, and to increase our understanding of how a simple system behaves when adding fluid to tissue.

MATERIALS AND METHODS

Inductance coil sensor and data collection system

The experimental system was built around a Foxfield N9923A Network Analyzer (Keysight, Santa Rosa, CA) connected to the induction coil sensor, by

single co-axial coil. The electrical circuit as well as photographs of the devices are shown in Figure 1. The induction coil sensor was made of a 240 mm diameter and 60 mm height plastic core cylinder with thickness of 1 mm. Copper electric wires used for transformer applications with cross-section of 1 mm^2 were wrapped in a single layer around the cylinder. The width of the wire wrapping (30 mm) and the coil are shown in the schematic in Figure 2. The network analyzer was connected to a laptop (Lenovo, Morrisville, NC) W541 through a LAN connection. The laptop collected and stored the data, using a simple C# program that we wrote based on Keysight's VISA library.

S_{21}, i.e., the ratio between the power entering port 2 to the power exit from port 1, was measured by the network analyzer throughout the experiment. We measured S_{21} for 50 frequencies equally spaced between 100 MHz and 1 GHz at a frequency of one measurement per 600 ms, with no averaging mode, IF bandwidth = 300 Hz, and maximum power level (5 dBm). The relation between S_{21} and the transmission impedance across the sensor coil is given by Keysight [2018]:

$$Z_T = Z_0 \frac{2 \cdot (1 - S_{21})}{S_{21}} \quad (1)$$

where Z_T is the transmission impedance of the induction coil at each excitation, and Z_0 is the system impedance in the absence of an excitation.

Internal bleeding simulation phantom

The phantom used to simulate the brain was similar to that used in previous studies for first-order experimental studies on internal bleeding in the brain [Lin and Clarke, 1982; González and Rubinsky, 2006]. It was a cylinder with a diameter of 160 mm and a height of 100 mm, made of a gel solution of 70% ethanol mixed with agar (35–40% ethanol, 60–65% water with agar [160 gr/L]). Internal bleeding was simulated with Standard 2-way Foley Balloon catheter (Bard, Covington, GA) with a rubber valve. The balloon was inserted in the gel at a height of 20 mm from the bottom of the gel. The balloons were placed at two locations relative to the center line, one at 10 ± 2 mm from the center line and the second at 10 ± 2 mm from the outer surface (see Fig. 2). The balloons were filled stepwise with physiological saline (0.9% NaCl in distilled water) to simulate internal bleeding. Precise quantities of saline were injected through the rubber valve with a 10 ml syringe (MedicPro, Kuala Lumpur, Malaysia).

Experimental method

S_{21} was measured and recorded continuously throughout the experiment. The experimental error in the S_{21} measurement was caused by several factors such as thermal noise and internal drift. A Faraday cylindrical cage, 250 mm diameter and 120 mm height, was built around the inductive coil sensor to reduce external sources of errors (Fig. 2). Experiments were performed to estimate the measurement error. In these experiments the coil was connected to the vector analyzer and surrounded by a Faraday cage. The instruments were calibrated in the same way they would be calibrated in the actual experimental simulations (i.e., no averaging, IF bandwidth = 300 Hz,

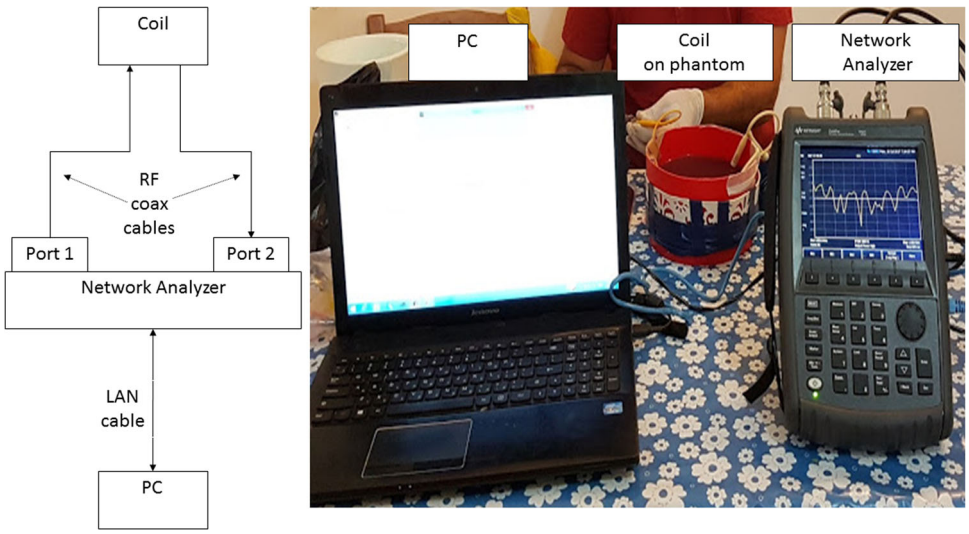

Fig. 1. Scheme of experimental electrical network and visualization of elements in the experiment.

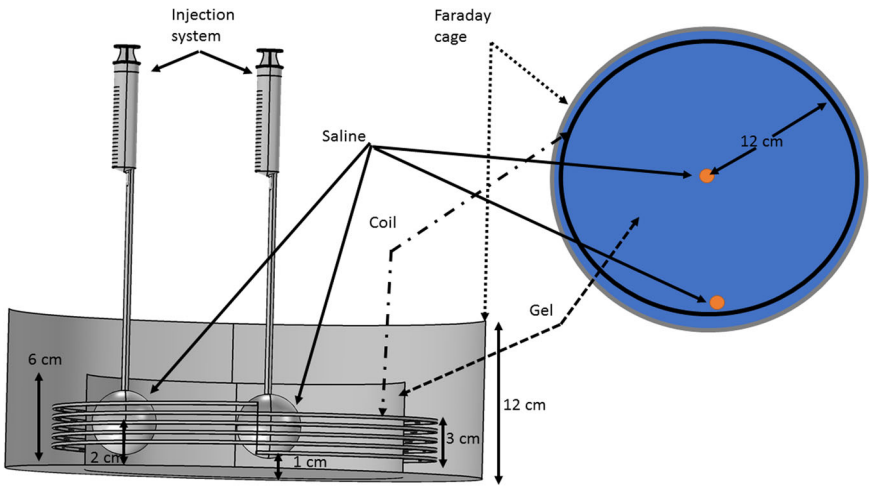

Fig. 2. Schematic of experimental design showing the location of the coils, gel, and saline injection sites.

maximum power level [5 dBm]). Twenty min of the S_{21} data were recorded with care to avoid any movement of the system. These experiments were performed under several different scenarios: (i) when the device was turned on for less than half an hour (cold device); (ii) when the device was turned on for more than 2 h (hot device); (iii) and with and without the phantom and repeated three times for each scenario. After verifying that the noise distribution was a normal one, we calculated the average (over the different measurements) and the standard deviation for the amplitude and phase. We estimated the relative error due to noise in the amplitude measurements to be 2.1e −4 dB and in the phase measurements to be 1e−3 deg. To overcome these systematic errors, we made numerous recurring measurements over time for the same experiment.

Internal bleeding was simulated by injecting precise volumes of saline into the balloon. The injections simulating the volume of blood in the brain were made in increments of 2 ± 0.2 ml. For every injected volume increment, we took between 30 and 60 S_{21} measurements during a period of at least 1 min. The injected volumes ranged from 0 to 10 ml. At least three experiments were made for each injected volume increment. Table 1 displays the dielectric properties of the phantom and saline as well the dielectric properties of the brain and blood.

Mathematical model for data analysis

To streamline data analysis, we defined the set of experimental results, $E(f,V,n)$, as follows:

$$E(f, V, n) = \{A(f, V, n), \phi(f, V, n)\} \qquad (2)$$

where f is the frequency at which the data were taken, V is the particular volume of blood in a particular experiment, n is the number of the measurement for that volume (between 30 and 60 recurring measurements were obtained for each volume data point), A is the amplitude, and ϕ is the phase. Equation (2) means that we are treating the amplitude and phase in the same way.

To simplify the analysis, we homogenized the results with respect to the average value

TABLE 1. Dielectric Parameters*

	Brain		Alcohol gel		Blood		Saline	
Frequency	ε_r	σ (S/m)	ε_r	σ (S/m)	ε_r	σ (S/m)	ε_r	σ (S/m)
100 MHz	89.76	0.79	53	0.55	76.8	1.23	120	1.48
500 MHz	53.82	1.08	51.9	5.5	63.3	1.38	61	1.51
1000 MHz	48.85	1.30	50	11	61.1	1.58	55	1.56

*The brain and the blood dielectric properties derived from [Hasgall et al., 2018]. The alcohol gel properties derived from [Megriche et al., 2012], where the water-agar phantom assumed to have the same dielectric properties as water. The saline dielectric properties derived from [Alanen et al., 1999].

$avg(E(f, V = 0))$, when the blood volume was zero, and normalized with respect to the maximal value of $E(f,V,n)$ in any measurement throughout one experimental series. This yields the variable, M:

$$M(f, V, n) = \frac{|E(f, V, n) - avg(E(f, V = 0))|}{max(|E(f, V, n) - avg(E(f, V = 0))|)} \quad (3)$$

Figure 3a shows typical results from an experiment in which the normalized and homogenized values of the amplitude and phase for the transmission impedance were measured at a frequency of 412.2 MHz (around the resonance), when saline was injected in a balloon in increments of 2–10 ml. The left panel shows the normalized and homogenized amplitude and phase as a function of the volume of the injected saline. The right panel shows a typical raw data distribution for the multiple measurements of the amplitude (top) and phase (bottom) in the first 2 ml increment. Analysis of the data points with one sample Kolmogorov–Smirnov test [Lilliefors, 1967] shows that the distribution is not normal ($P < 0.05$). For comparison, Figure 3 shows a normal distribution fit over the non-normal distribution of the data for the amplitude and phase.

In the next step, we wanted to define a statistical parameter for the sensitivity of each frequency to an injection of 2 ml, so we wanted to use a test that would measure if the change in the amplitude/phase following each injection was significant. Since our distribution was not normal, we used the two-sample Kolmogorov–Smirnov Test (TSKMT) to determine if the data from two tested groups originate from the same distribution. This test is particularly important for experimental results such as those in Figure 4 (explained in detail in the Results section), for frequencies of 412 and 338 MHz, where it is not obvious how to identify different distributions.

We defined the results of the TSKMT test (marked by, $h(f,m)$) to be 0 when two groups of data that were compared were from the same distribution and 1 when the two groups of data were from different distributions. We also calculated the average value of $M(f, V)$ and the standard deviation (std).

To evaluate the frequency-dependent sensitivity of the measurements to increments in volume of injected fluid, we defined the ratio of the measurements between two sequential volumes of injected fluid, m and $m+1$; $V(m)$ and $V(m+1)$, as:

$$R(f, m) = \frac{|avg(M(f, V(m))) - avg(M(f, V(m+1)))|}{max(std(M(f, V(m))), std(M(f, V(m+1))))} \quad (4)$$

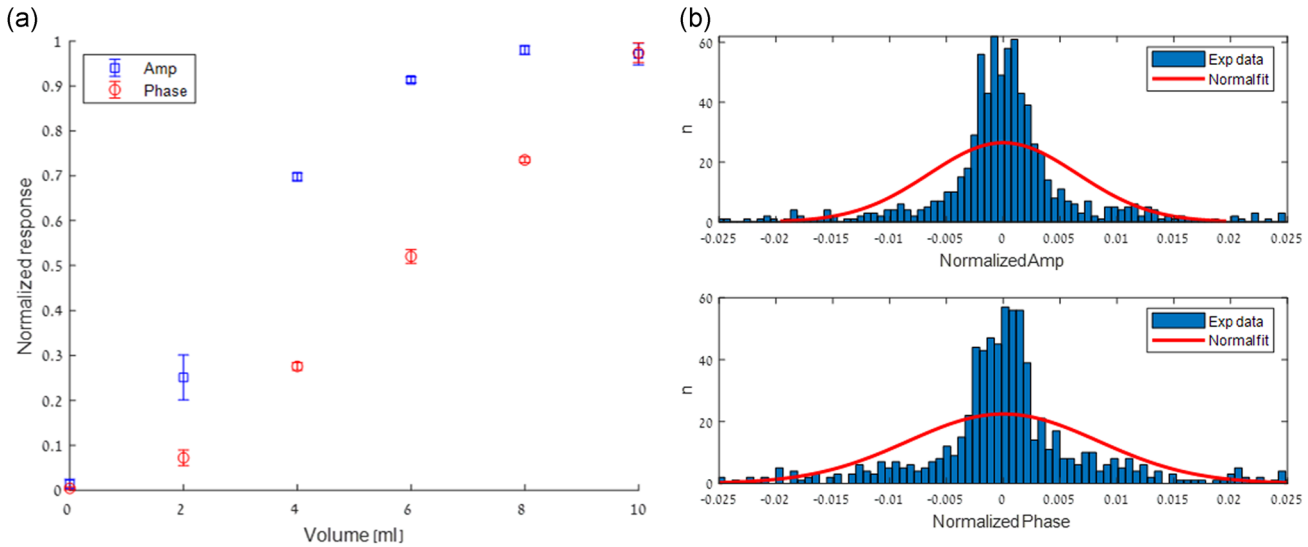

Fig. 3. (**a**) Normalized and homogenized amplitude and phase as a function of the volume of saline injected into the phantom's center, measured at a frequency of 412.2 MHz (around the resonance). Due to manual injection we have between 30 and 60 recurring measurements for each volume data point. The results are given as mean ± SD. (**b**) Example of non-normal distribution of the data. Typical raw data distribution for measurements in one volume increment of the first 2 ml injection. A normal distribution plot is shown, for comparison of the amplitude (top) and phase (bottom).

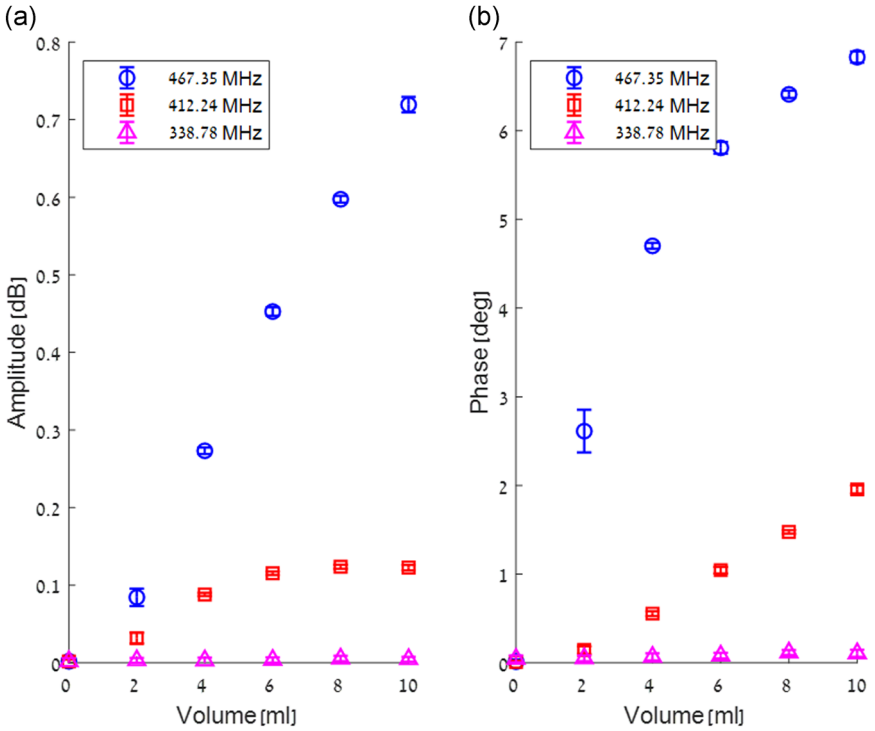

Fig. 4. Examples of the changes in impedance (**a**) and phase (**b**) in response to incremental increase in the volume of injected saline at the center of the phantom, as a function of three different arbitrary chosen frequencies. The results are given as mean ± SD.

where $R(f,m)$ is a measure of how many standard deviations are between two subsequent injected volumes in our experiments, at a certain frequency.

We now define $r(f, m)$ as a Boolean function in the following way:

$$r(f,m) = \begin{cases} 1 & \text{if } R(f,m) \geq 2 \\ 0 & \text{else} \end{cases} \quad (5)$$

We defined two parameters to define the frequency-dependent sensitivity of the measurements to changes in volume. One parameter provides information on how many times the value of $M(f)$ changes in a statistically significant manner during a series of experiments in which the volume of the injected fluid has increased in controlled increments from $V = 0$ to $V = V_{\max}$.

$$Num(f) = \sum_m h(f,m) \cdot r(f,m) \quad (6)$$

The summation is over all the discrete changes in volume. In Equation (6), $h(f,m)$ is the Boolean function defined in regards to the TSMKT test. Here, $h(f,m)$ takes the value 1 when two adjacent sequential measurements belong to two different distributions, and takes the value 0 when the statistical analysis shows that they belong to the same standard distribution. We consider measurements at two consecutive changes in volume to be of statistical significance only in situations in which the difference in mean values is at least two standard deviations ($P < 0.05$).

The second parameter is a measure of the number of standard deviations between volume measurements for a particular frequency. It is a measure of the sensitivity of the measurements at one frequency. This is given by:

$$grade(f) = \sum_m h(f,m) \cdot r(f,m) \cdot R(f,m) \quad (7)$$

It is useful to notice that the criteria in (6, 7) are expressed only in terms of values obtained from the statistical analysis; i.e., whether two sets of measurements belong to the same distribution and number of standard deviations between the averages of two sets of measurements.

This study produced thousands of data points. The mathematical model was designed to facilitate

a statistically robust means to analyze experimental data of the kind generated by this experimental system.

Numerical simulation method

To test the effect of the Faraday cage on the frequency range, we reproduced the simulations we performed in Oziel et al. [2018]. In brief, we used the COMSOL RF Module Version 5.2. The simulation used a complete anatomical model of a head and brain. We classified the brain elements into four types of tissue: white matter, gray matter, cerebrospinal fluid, and the skull bone. For each brain's element, we coupled the appropriate electrical properties (Permittivity and Conductivity) per frequency using ITIS's dielectric tissue properties database [Hasgall et al., 2018]. The model includes a coil made of 16 turns of copper wire with a diameter of 240 mm and height of 30 mm.

RESULTS

Typical experimental results are shown in Figure 4. The figure shows the (non-normalized) change in impedance (left) and phase (right) as a function of the incremental increase in the volume of injected saline at the center of the phantom at three different arbitrary frequencies that respond differently to the same injection. Up to 60 measurements were taken for each incremental increase in volume, and the figure shows the data points as they were taken sequentially in time. The results are typical of all experiments. They show that the measurements are strongly frequency-dependent and that at some frequencies the resolution is excellent while at others the increase in injected volume cannot be detected. The resolution for a frequency of 467.35 MHz is excellent (Num = 5 and high grade). The effects of changes in volume on changes in amplitude and phase are well distinguished and evident. Obviously, this frequency has a change in volume detection resolution of at least 2 ml. However, the resolution of an adjacent frequency of 412.24 MHz is poor (Num = 3 and low grade). It generates changes in amplitude that could discriminate in a volume resolution of 4 ml at best. At a frequency of 338.78 MHz, the change in volume of saline produces no discernible effect (Num = 0). It is obvious that inductive coils can be used to detect changes in saline volume; however, the resolution is strongly frequency-dependent.

Use of the statistical model to analyze the internal bleeding phantom simulation experiment

Figure 5 gives the results of the statistical analysis for all experiments, repeats, and frequencies and injection locations. The top panel was derived from Equation (6) and is a histogram that gives the percentage from all the experiments in this study in which a certain value of Num was calculated. Since there are five increments in the volume of injected fluid, the values of Num can range from 0 to 5. The top panel shows that for 11% of the tested frequencies Num = 5; i.e., at those frequencies increments in injected volume can be detected with a statistical significance of $P < 0.05$ for all five consecutive injection increments of 2 ml. The top panel shows that for 26% of the frequencies it is possible to detect with a statistically significant resolution that there is a statistically significant distinction of four (15%) or five (11%) injections. In 12% of the frequencies Num = 0; i.e., it is impossible to detect the changes in injected volume.

When using the same technique to calculate Num for a (single) increment of 10 ml (i.e., from 0 to 10 ml), we found that there are 22 frequencies that can detect the injected volume with a statistically significant resolution. Obviously, the lower the resolution required for detection of changes in volume, the larger the number of frequencies that can detect these changes with high statistical significance.

Concerning the actual value of the resolution of the measurements, for all the frequencies for which Num = 5, the value of the measured impedance amplitude in 90% of the measurements ranged from 0.141 to 0.228 ohm. For Num = 4, the value of the impedance amplitude in 90% of the measurements ranged from 0.082 to 0.105 ohm. The middle panel in Figure 5 displays the average value of Num(f) calculated from Equation (6), as a function of the frequency. The amplitude is marked blue, and the phase red. The panel shows that there is no frequency with Num = 5, in all the experiments. The maximal value of Num is 4.42 at 427 MHz. No clear pattern for the Num value, dependence of frequency was observed. In other words, there are some frequencies that have a value of Num = 5 for many cases. However, even in these frequencies, there are cases in which not even a single injection was recognized. Interestingly, the lack of recognition of a single injection can occur at any stage of the injection sequence. This illustrates the importance of multifrequency measurements.

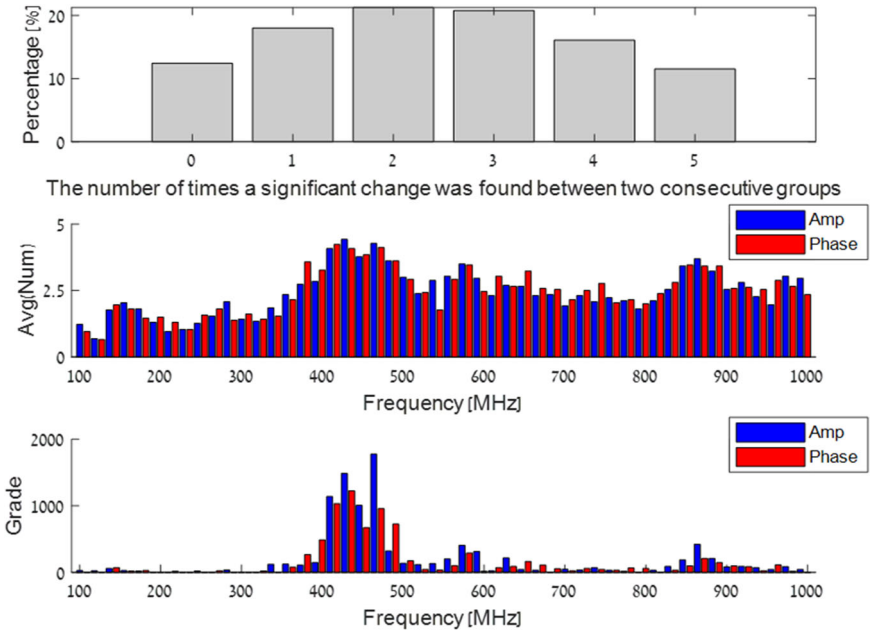

Fig. 5. **Top panel**: Histogram that gives the percentage of experiments in this study in which a certain value of Num was calculated. **Middle panel**: Average value of Num(*f*). **Bottom panel**: Value of *grade*(*f*); i.e., provides a measure of the sensitivity in detecting changes in injected volume at each frequency.

Amplitude-phase correlation

The bottom panel in Figure 5 suggests that there is a correlation between the changes in amplitude and phase at frequencies with a high grade. Next, we explored the correlation coefficients between amplitude and phase in the experiments of this study. Changes in impedance due to changes in the volume of saline can be written as:

$$\Delta Z = abs\left(f_1\left(real\left(Z_{V_2} - Z_{V_1}\right)\right) + f_2\left(imag\left(Z_{V_2} - Z_{V_1}\right)\right)\right) \quad (8)$$

The injected volume at which the base line reading of the impedance is taken is marked as (V_1). The second volume is (V_2). The changes in impedance between V_1 and V_2 are a result of the changes in amplitude and phase of the current flowing through the coil, due to changes in the volume of the injected saline (representing blood), where f_1 and f_2 are any arbitrary functions that enable aligning the impedance units correctly. In our previous simulations [Oziel et al., 2018], we used the following expression for the change in impedance with a change in volume:

$$\Delta Z = abs\left(Z_{V_2} - Z_{V_1}\right) \quad (9)$$

This expression contains an implicit assumption that there is a high correlation between amplitude and phase, and that the amplitude and phase have an equal weight. Our experimental results allow us to precisely evaluate the correlation coefficients between amplitude and phase, using Hall [2015]:

$$[R_i(f), p_i(f)] = crossCoef\left(amp_i(f), phase_i(f)\right) \quad (10)$$

Where amp and phase vectors were normalized using Equation (3), i is the experiment index, f is the frequency, $R_i(f)$ is the correlation coefficient for the specific measurement, i, and frequency, f, and $p_i(f)$ are the P-value which tests the hypothesis; i.e., $P < 0.05$ means that the correlation R is conclusive. Figure 6 shows several correlations between changes in amplitude and phase from arbitrary frequencies calculated from the experimental data.

Figure 7 is a histogram that shows the frequencies at which the cross-correlation gives $R > 0.9$ and $p < 0.05$ for all the cases in which Num > 3. Comparing Figure 7 with the bottom panel of Figure 5 shows that for frequencies in which the statistical value grade is high, there is a high cross-correlation between amplitude and phase.

We summarized the calculated correlations from all the experiments and found that the percentage of all frequencies in which the correlation between the changes in amplitude and phase are good ($R > 0.9$ and

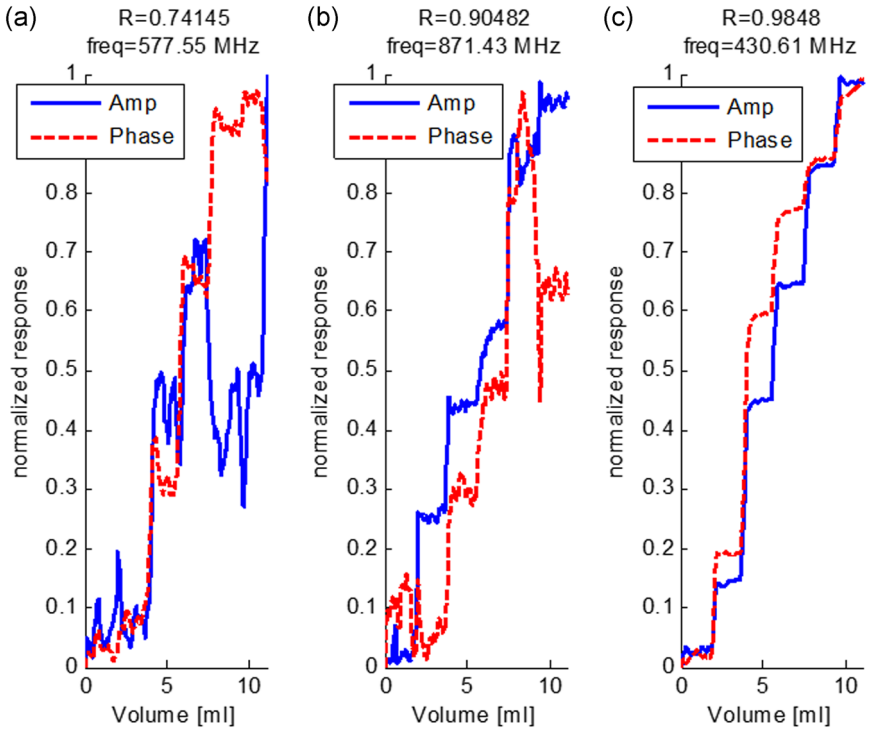

Fig. 6. Examples of different correlations: $R = 0.74$ (**a**), $R = 0.90$ (**b**) and $R = 0.98$ (**c**), between changes in amplitude and phase calculated from the experimental data. The graphs were chosen as examples for three different correlation coefficients.

$p < 0.05$) is 24.88%, bad ($R < 0.9$ and $p < 0.05$) is 62.20%, and the other ($p > 0.05$) is 12.92%. In a substantial percentage of frequencies, the correlation is good. As mentioned earlier, the good correlations occur at frequencies at which the grade value is high.

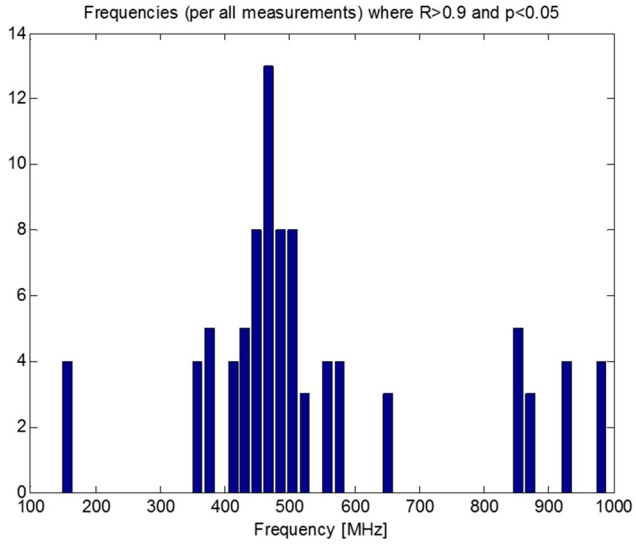

Fig. 7. Histogram showing the frequencies at which the *cross-correlation* gives $R > 0.9$ and $p < 0.05$ for all the cases in which Num > 3.

We used the observation concerning the correlation to improve the resolution of our measurements. We will next show how a linear combination of amplitude and phase can lead to higher sensitivity for detection of changes in blood volume/tissue ratio. We can define the function G as:

$$G(f, V, n) = \frac{(A(f, \hat{V}, n) + \varnothing(f, \hat{V}, n))}{2} \quad (11)$$

where A is the amplitude vector, $\varnothing$ is the phase vector, and the operator ^ is the normalization operator defined in Equation (3). Accordingly, Equation (4) becomes:

$$R(f, m) = \frac{|avg(G(f, V(m))) - avg(G(f, V(m+1)))|}{max\,(std(G(f, V(m))), std(G(f, V(m+1))))} \quad (12)$$

The results are shown in Figure 8. Figure 8 is actually a modified version of the bottom panel of Figure 5 to which we have added the grade value for the combination amplitude and phase from

Equation (11). It is evident that in all the frequencies that had a strong response (high resolution) to changes in saline/tissue ratio (i.e., showed a high correlation between phase and amplitude), the values of the combination grade are higher than the value of the grade for amplitude and phase alone. This suggests that the combination of amplitude and phase yields higher resolution results at optimal frequencies.

Effect of the location of the saline injection on measurement resolution

It is obviously of substantial interest to understand the effects of the location of the blood hematoma (saline injection in the gel) on the resolution of the measurements and frequencies that give the highest resolution. To this end, we analyzed the experiments separately in which the balloon was close to the center and those in which the balloon was close to the margin (Fig. 9). The panels show the frequency-dependent percentage at which Num = 5 for the combination phase and amplitude at the two locations of the balloon. It is interesting to note that the highest resolution frequencies are different between the two locations of the balloon.

Effect of the boundary conditions

To verify the effects of the boundary conditions, we reproduced the simulations in Oziel et al. [2018] with Faraday cage boundary conditions. Figure 10 was obtained from a numerical simulation similar to that in Oziel et al. [2018], albeit with Faraday cage boundary conditions, in which we injected 9 ml physiological saline in 30 equal increments in an alcohol gel. The figure gives the ratio between the saline injections that caused a change in impedance at 500 MHz to the change in impedance at 1,000 MHz (the frequencies tested in Oziel et al. [2018] are shown in blue circles) or the ratio between 430 and 870 MHz (the highest frequencies from the present study are shown in red squares). The ratio between the changes in impedance for both ratios was between 1.5 and 3 times. This demonstrates that the effect of the Faraday cage is to enhance the resolution in the frequencies around 500 MHz over that in the 1,000 MHz range. This means that as the frequency increases, in case of absorption boundary conditions, the sensitivity to the injection would also increase. After adding a Faraday cage, the most sensitive frequencies were at the center of the frequency range (approximately 430 MHz).

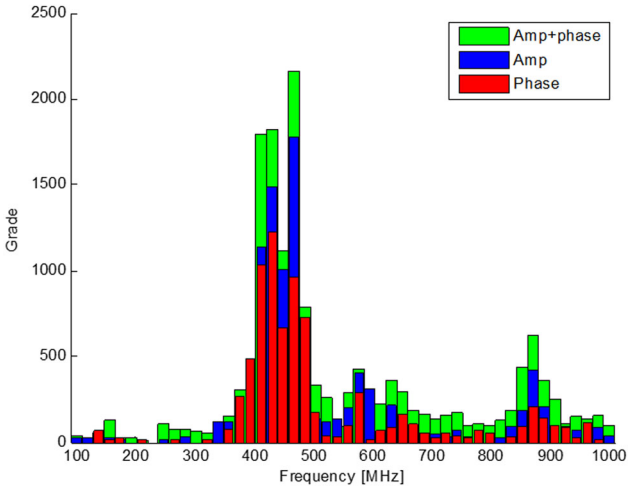

Fig. 8. Comparison between the grade value for change in amplitude, change in phase, and linear combination of change in phase and change in amplitude, as a function of frequency.

DISCUSSION

This first-order experimental study on the use of an inductive coil around the head, for the detection of changes in volume of saline injected in a phantom of the head, supports the results in our previous study that this simple technology has the potential to detect changes in the volume of blood in the head in a hematoma with high resolution [Oziel et al., 2018]. It also shows that the resolution is frequency-dependent, which was also predicted by our recent theoretical study [Oziel et al., 2018]. To get a handle on the significance of the multifrequency measurements, we developed a method to statistically analyze the data. In the ensuing discussion, we will illustrate its use with the results emerging from these experiments. It should be emphasized that we did not try to develop a diagnostic algorithm, but rather a way to analyze multifrequency data of a type that will most likely emerge from the use of a single inductive coil to detect changes in the volume of a hematoma in the head.

The goal of this study was to examine the effect of frequency on the ability to detect internal bleeding in the head, in a range of frequencies that was not studied before, between the typical beta dispersion frequencies of tissue and low microwave frequencies. Earlier studies of this kind examined frequencies in the range from 1 MHz to below 400 MHz [e.g., González et al., 2013; Li et al., 2019] or above 1 GHz [Lin and Clarke 1982; Mobashsher and Abbosh, 2016]. The lower range of frequencies was chosen in earlier studies of this kind because it was thought that the measurement sensitivity would be greater in the beta dispersion range and slightly above, and because of deficiencies in modeling the entire set

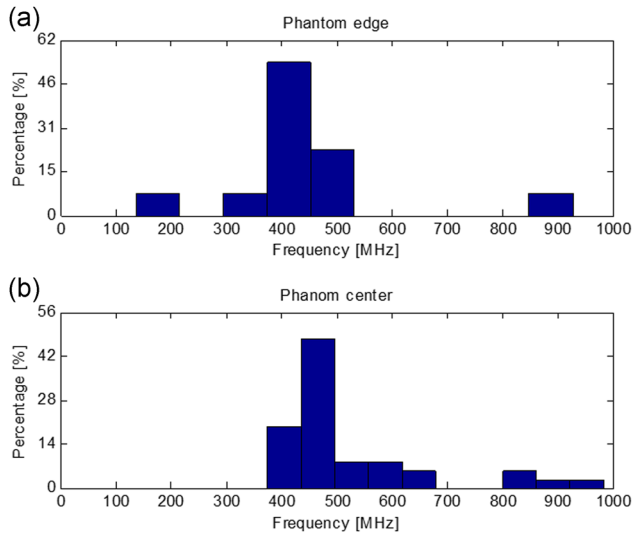

Fig. 9. Frequency-dependent percentage at which Num = 5 for the combination of phase and amplitude at the two locations: The phantom edge (**a**) and the phantom center (**b**), of the saline injection.

of Maxwell equations at higher frequencies (the simplified Maxwell equations fail above about 400 MHz). The other studies examined low microwave frequencies from 1 to 3 GHz, probably because this is the range of what is usually defined as low microwave frequencies [Lin and Clarke 1982; Mobashsher and Abbosh, 2016]. Our numerical studies of the complete Maxwell equations in an anatomically complete 3D model of a head suggested

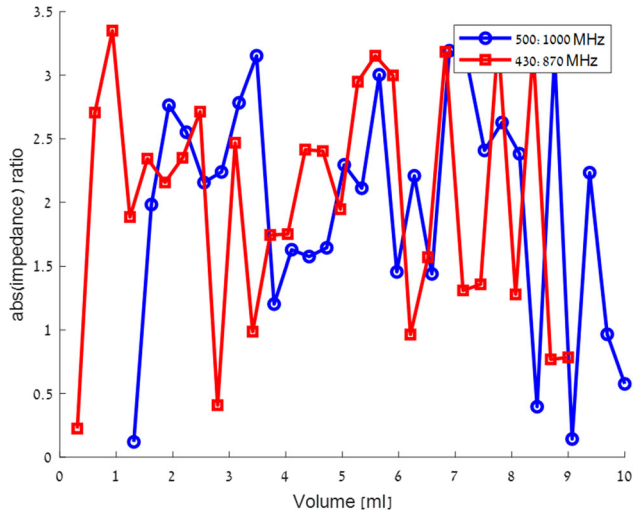

Fig. 10. Results from a numerical simulation with Faraday boundary conditions. The figure gives the ratio between impedance changes induced by saline injections that caused a change in impedance at 500 MHz to the change in impedance at 1,000 MHz (blue circles) and the impedance ratio between 430 and 870 MHz (red squares).

that frequencies in the intermediate range from 100 MHz to 1 GHz may be valuable for the detection of internal bleeding in the head [Oziel et al., 2017; Oziel et al., 2018]. Indeed, the results of this experimental study show that sensitivity to changes in blood volume in the range of frequencies from 400 to 600 MHz is higher than sensitivity at frequencies lower than 300 MHz (Fig. 8). Also, sensitivity in the range of frequencies from about 800 to 900 MHz is higher than sensitivity at 1 GHz (Fig. 8). Obviously, the study of the range of frequencies examined in this paper can provide valuable information for the design of internal bleeding detection devices. We believe that in the future, when learning algorithms will be applied to clinical data from a broad range of frequencies, it will be found that every range of frequencies can provide additional information on the nature as well as the location of the hematomas, similar to what was found in González et al. [2013].

Effect of the boundary conditions

The bottom panel of Figure 5 displays the value of grade(f), calculated from Equation (7) as a function of the frequency; grade(f) provides a measure of the sensitivity in detecting changes in injected volume at each frequency. The values for amplitude and phase are in blue and red, respectively. The bottom panel demonstrates that, quantitatively, not all frequencies respond the same way to changes in the injected volume of saline. In fact, at frequencies lower than 350 MHz the resolution is too low to detect changes in the simulated fluid/brain tissue ratio of our experiments. Also, similar to previous theoretical studies, the highest resolution detection peak is in the frequency range of 390 to 500 MHz with two lower peaks at 570 and 870 MHz. While the results of the experimental studies concerning the high-resolution frequency peaks are qualitatively the same as in the theoretical study [Oziel et al., 2018], the results are quantitatively different. In the theoretical study, we found that the higher the frequency the higher the resolution, while in this study we found that the peak at 880 MHz was substantially lower than at 450 MHz. We showed that the difference is due to different boundary conditions in the experimental and theoretical studies. In the theoretical study, we used absorption boundary conditions. In the experiment, we used a Faraday cage to minimize reflection from the surroundings. This causes standing waves and substantially changes the response at different frequencies.

This part of the study also illustrates the importance of boundary conditions in the experiments

and the sensitivity of the results to the boundary conditions. A practical conclusion is that Faraday cages may be needed around the single coil inductive sensor. The Faraday cage can significantly limit a real device and there is a need to find creative solutions to design or overcome the need for a cage. A possible solution is the use of a mask similar to the mask used in radiotherapy, which can block the reflection from the environment as well as fix the coil so it will not move.

Effect of the location of the injections

We showed (Fig. 9) how the sensitivity of high/low frequencies vary depending on the location of the injection (center and phantom margin). However, the frequencies in the center of the frequency range showed the highest sensitivity for both injection locations. It appears that both the high and low frequencies are superfluous. On the other hand, we believe that these frequencies contain important information that can help in designing a clinical algorithm to identify the location of the bleeding. However, it is clear that for a device designed only to detect changes in blood/tissue ratio, there is no need to scan the whole frequency range. In addition, it appears that having to scan the frequency range between 100 MHz and 1 GHz limits the device in both the need to support a greater frequency space and in the sampling time. However, our measurement device (FoxField N99923A; Keysight) has the ability to measure this range in less than 650 ms, thereby overcoming the limitation of the sampling time.

CONCLUSIONS

The primary goal of this study was an initial validation of our theoretical study on the use of a single inductive coil around the head for the detection of internal bleeding [Oziel et al., 2018]. Because of the complexity of the results, and to facilitate a better analysis of the experimental results, we derived a statistically based mathematical method of analysis. This approach may have value in the future for the analysis of experiments performed in vivo. We believe that other scientific fields may also benefit from this approach.

Our analysis reveals that the experimental results are consistent with the results obtained in the previous numerical simulation [Oziel et al., 2018]. We found that the inductive coils can detect changes in injected saline volume as low as 2 ml, the resolution is frequency-dependent, and the statistical analysis can point to frequencies with the highest resolution. We used a Faraday cage to avoid reflection back to the coil from the surrounding environment and showed that the boundary conditions have a large impact on frequency sensitivity. We examined the correlation between the amplitude and phase and found that there is a high correlation between amplitude and phase for frequencies with high grade. This knowledge can help to enhance frequency resolution and also be used for choosing optimal frequencies for a future clinical algorithm. Finally, we believe that there is important information at the high frequencies (at approximately 1 GHz) that may help locate the position of the bleeding.

While the goal of this study was to provide first-order experimental support to the numerical analysis, and the mathematical analysis was restricted to generate a better understanding of the results of these experiments, the findings and in particular the statistical model may help in the future development of a clinical diagnostic algorithm using a simple single coil inductive system for monitoring bleeding in the brain.

ACKNOWLEDGMENT

This work is based on a portion of a dissertation to be submitted by Moshe Oziel in partial fulfillment of the requirements for a PhD degree to Tel-Aviv University.

REFERENCES

Alanen E, Lahtinen T, Nuutinen J. 1999. Penetration of electromagnetic fields of an open-ended coaxial probe between 1 MHz and 1 GHz in dielectric skin measurements. Phys Med Biol 44:N169–N176.

An SJ, Kim TJ, Yoon BW. 2017. Epidemiology, risk factors, and clinical features of intracerebral hemorrhage: an update. J Stroke 19:3–10.

Caceres JA, Goldstein JN. 2012. Intracranial hemorrhage. Emerg Med Clin North Am 30:771–794.

Clarke MJ, Lin JC. 1983. Microwave sensing of increased intracranial water content. Invest Radiol 18:245–248.

Foster KR, Schwan HP. 1989. Dielectric properties of tissues and biological materials: a critical review. Crit Rev Biomed Eng 17:25–104.

Foundation Brain Aneurism. 2018. Brain aneurysm statistics and facts. Available from https://www.bafound.org/about-brain-aneurysms/brain-aneurysm-basics/brain-aneurysm-statistics-and-facts/ [Last accessed 12 May 2018].

Gabriel C. 2000. *The Dielectric Properties of Tissues.* Dordrecht: Springer. pp 75–84.

Gebel JM, Sila CA, Sloan MA, Granger CB, Weisenberger JP, Green CL, Topol EJ, Mahaffey KW. 1998. Comparison of the ABC/2 estimation technique to computer-assisted volumetric analysis of intraparenchymal and subdural hematomas complicating the GUSTO-1 trial. Stroke 29:1799–1801.

Geneva World Health Organization Estimates. 2016. Global Health. Available from http://www.who.int/healthinfo/global_burden_disease/en/ [Last accessed 12 May 2018].

González CA, Blumrosen G, Rubinsky B. 2010. Remote monitoring of internal bleeding based on magnetic induction and cellular phone technology: a potential application in poor regions in México. Computación Y Sistemas 14:187–195.

González CA, Rubinsky B. 2006. A theoretical study on magnetic induction frequency dependence of phase shift in oedema and haematoma. Physiol Meas 27:829–838.

González CA, Valencia JA, Mora A, Gonzalez F, Velasco B, Porras MA, Salgado J, Polo SM, Hevia-Montiel N, Cordero S, Rubinsky B. 2013. Volumetric electromagnetic phase-shift spectroscopy of brain edema and hematoma. PloS One 8:e63223.

Griffiths H, Stewart WR, Gough W. 1999. Magnetic induction tomography: a measuring system for biological tissues. Ann N Y Acad Sci 873:335–345.

Hall G. 2015. Pearson's correlation coefficient. Other words, 1(9). Available from http://www.hep.ph.ic.ac.uk/~hallg/UG_2015/Pearsons.pdf [Last accessed 12 May 2018].

Hasgall PA, Di Gennaro F, Baumgartner C, Neufeld E, Lloyd B, Gosselin MC, Payne D, Klingenböck A, Kuster N. 2018. IT'IS Database for thermal and electromagnetic parameters of biological tissues. Version 4.0. Available from http://itis.swiss/database [last accessed 8 October 2019].

Haynes M, Stang J, Moghaddam M. 2014. Real-time microwave imaging of differential temperature for thermal therapy monitoring. IEEE T Bio-Med Eng 61:1787–1797.

Huisman TA. 2005. Intracranial hemorrhage: ultrasound, CT and MRI findings. Eur Radiol 15:434–440.

Keysight. 2018. Converts the S21 into the transmission impedance (Zt). Available from https://www.keysight.com/main/editorial.jspx?ckey=1536926&id=1536926&nid=-11143.0.00&lc=eng&cc=CA [Last accessed 12 May 2018].

Li G, Chen J, Gu S, Yang J, Chen Y, Zhao S, Xu J, Bai Z, Ren J, Xu L, Chen M. 2019. A dual parameter synchronous monitoring system of brain edema based on the reflection and transmission characteristics of two-port test network. IEEE Access 15:50839–50848.

Lilliefors HW. 1967. On the Kolmogorov-Smirnov test for normality with mean and variance unknown. J Am Stat Assoc 62:399–402.

Lin JC, Clarke MJ. 1982. Microwave imaging of cerebral edema. Proc IEEE 70:523–524.

Little RD. 2008. Increased intracranial pressure. Clin Pediatr Emerg Med 9:83–87.

Megriche A, Belhadj A, Mgaidi A. 2012. Microwave dielectric properties of binary solvent wateralcohol, alcohol-alcohol mixtures at temperatures between -35°C and +35°C and dielectric relaxation studies. Mediterr J Chem 1:200–209.

Mobashsher AT, Abbosh AM. 2016. On-site rapid diagnosis of intracranial hematoma using portable multi-slice microwave imaging system. Sci Rep 6:37620.

Nyboer J. 1970. Electrorheometric properties of tissues and fluids. Ann N Y Acad Sci 170:410–420.

Oziel M, Hjouj M, Gonzalez CA, Lavee J, Rubinsky B. 2016. Non-ionizing radiofrequency electromagnetic waves traversing the head can be used to detect cerebrovascular autoregulation responses. Sci Rep 6:21667.

Oziel M, Korenstein R, Rubinsky B. 2017. Radar based technology for non-contact monitoring of accumulation of blood in the head: a numerical study. PloS One 12:e0186381.

Oziel M, Korenstein R, Rubinsky B. 2018. Non-contact monitoring of temporal volume changes of a hematoma in the head by a single inductive coil: a numerical study. IEEE T Bio-Med Eng 66:1328–1335.

Qureshi AM, Mustansar Z, Mustafa S. 2018. Finite-element analysis of microwave scattering from a three-dimensional human head model for brain stroke detection. R Soc Open Sci 5:180309.

Rao CPV, Bershard EM, Calvillo E, Maldonado N, Damani R, Mandayam S, Suarez JI. 2018. Real-time noninvasive monitoring of intracranial fluid shifts during dialysis using volumetric integral phase-shift spectroscopy (VIPS): a proof-of-concept study. Neurocrit Care 28:117–126.

Scharfetter H, Ninaus W, Puswald B, Petrova GI, Kovachev D, Hutten H. 1999. Inductively coupled wideband transceiver for bioimpedance spectroscopy (IBIS). Ann N Y Acad Sci 873:322–334.

Teichmann D, Foussier J, Jia J, Leonhardt S, Walter M. 2013. Noncontact monitoring of cardiorespiratory activity by electromagnetic coupling. IEEE Trans Biomed Eng 60:2142–2152.

Teichmann D, Kuhn A, Leonhardt S, Walter M. 2014. The main shirt: a textile-integrated magnetic induction sensor array. Sensors (Switzerland) 14:1039–1056.

Wadley HNG, Choi BW. 1997. Eddy current determination of the electrical conductivity-temperature relation of Cd1-xZnxTe alloys. J Cryst Growth 172:323–336.